THYROID
Volume 26, Number 10, 2016

DOI: 10.1089/thy.2016.0106

Overexpression of Interleukin-4 in the Thyroid of Transgenic Mice Upregulates the Expression of *Duox1* and the Anion Transporter Pendrin

Zineb Eskalli,[1] Younes Achouri,[2] Stephan Hahn,[3] Marie-Christine Many,[4] Julie Craps,[4] Samuel Refetoff,[5] Xiao-Hui Liao,[5] Jacques E. Dumont,[1] Jacqueline Van Sande,[1] Bernard Corvilain,[6] Françoise Miot,[1] and Xavier De Deken[1]

Background: The dual oxidases (Duox) are involved in hydrogen peroxide generation, which is essential for thyroid hormone synthesis, and therefore they are markers of thyroid function. During inflammation, cytokines upregulate *DUOX* gene expression in the airway and the intestine, suggesting a role for these proteins in innate immunity. It was previously demonstrated that interleukin-4 (IL-4) upregulates *DUOX* gene expression in thyrocytes. Although the role of IL-4 in autoimmune thyroid diseases has been studied extensively, the effects of IL-4 on thyroid physiology remain largely unknown. Therefore, a new animal model was generated to study the impact of IL-4 on thyroid function.
Methods: Transgenic (Thyr-IL-4) mice with thyroid-targeted expression of murine IL-4 were generated. Transgene expression was verified at the mRNA and protein level in thyroid tissues and primary cultures. The phenotype of the Thyr-IL-4 animals was characterized by measuring serum thyroxine (T4) and thyrotropin levels and performing thyroid morphometric analysis, immunohistochemistry, whole transcriptome sequencing, quantitative reverse transcription polymerase chain reaction, and *ex vivo* thyroid function assays.
Results: Thyrocytes from two Thyr-IL-4 mouse lines (#30 and #52) expressed IL-4, which was secreted into the extracellular space. Although 10-month-old transgenic animals had T4 and thyrotropin serum levels in the normal range, they had altered thyroid follicular structure with enlarged follicles composed of elongated thyrocytes containing numerous endocytic vesicles. These follicles were positive for T4 staining the colloid, indicating their capacity to produce thyroid hormones. RNA profiling of Thyr-IL-4 thyroid samples revealed modulation of multiple genes involved in inflammation, while no major leukocyte infiltration could be detected. Upregulated expression of *Duox1*, *Duoxa1*, and the pendrin anion exchanger gene (*Slc26a4*) was detected. In contrast, the iodide symporter gene *Slc5a5* was markedly downregulated resulting in impaired iodide uptake and reduced thyroid hormone levels in transgenic thyroid tissue. Hydrogen peroxide production was increased in Thyr-IL-4 thyroid tissue compared with wild-type animals, but no significant oxidative stress could be detected.
Conclusions: This is the first study to show that ectopic expression of IL-4 in thyroid tissue upregulates *Duox1*/*Duoxa1* and *Slc26a4* expression in the thyroid. The present data demonstrate that IL-4 could affect thyroid morphology and function, mainly by downregulating *Slc5a5* expression, while maintaining a normal euthyroid phenotype.

Introduction

Follicular units are critical for the principal function of the thyroid gland: iodide concentration for biosynthesis and secretion of the thyroid hormones triiodothyronine (T3) and thyroxine (T4). Iodide uptake is supported by the Na^+/I^- symporter (NIS) that localizes to the basolateral membrane of follicular cells, while apical iodide efflux is mediated by the recently characterized Ca^{2+}-activated ion channel anoctamin-1 (1,2) and the anion exchanger pendrin encoded by *SLC26A4* (3). Within the lumen, iodide binding to tyrosine residues on thyroglobulin (Tg) is catalyzed by thyroperoxidase (TPO) after oxidation of iodide by hydrogen peroxide (H_2O_2) (4). The thyroid H_2O_2-generating system is composed of the dual oxidases, Duox1 and Duox2, which are membrane-bound NADPH-dependent flavoproteins (5,6).

[1]Institut de Recherche Interdisciplinaire en Biologie Humaine et Moléculaire (IRIBHM); [3]Laboratory of Image, Signal processing and Acoustics—Brussels School of Engineering; Université libre de Bruxelles (ULB), Brussels, Belgium.
[2]Institut De Duve; [4]Pôle de Morphologie (MORF); Université Catholique de Louvain (UCL), Brussels, Belgium.
[5]Department of Medicine, University of Chicago, Chicago, Illinois.
[6]Department of Endocrinology, ULB-Hôpital Erasme, Brussels, Belgium.

These Ca^{2+}-activated NADPH oxidases require additional factors, the DuoxAs, for appropriate maturation and translocation to the apical pole of the thyrocyte (7,8). The *thyd* mouse carries a biallelic *Duox2* inactivating mutation, which results in a profound iodide organification defect, In contrast, *Duox1* KO mice remain euthyroid (9,10). Complete inactivation of the *Duoxa1* and *Duoxa2* genes results in growth retardation and hypothyroidism that are related to the absence of correct Duox maturation (11). Mutations in *DUOX2* and *DUOXA2* in humans cause inherited hypothyroidism, and emphasize the functional importance of these proteins in thyroid hormonogenesis (12,13).

During thyroid embryogenesis, *Duox* expression emerges only during the late stages of cell differentiation when the follicular structure has developed (14,15). In rat thyroid cell lines, Pax8-mediated induction of *Duox2* expression and increased *Duox1* expression after functional inactivation of Nkx2.1 have been demonstrated (16,17). However, no significant thyrotropin (TSH)-dependent modulation of *DUOX* transcription has been shown in humans and mice (14,18). The thyroid oxidases are considered as essential thyroid-related markers, but they are not thyroid-specific genes. Duox protein expression has been documented on the luminal side of highly differentiated epithelia (e.g., airway, salivary glands, and intestinal tract), where these proteins play a potent role in innate host defense (19). During infection or chronic inflammation, cytokines secreted by helper T lymphocytes (Th)2 (IL-4 and IL-13) or Th1 (IFN-γ) increase *DUOX1* or *DUOX2* expression levels (20–22). In human thyrocytes, it has been demonstrated *in vitro* that IL-4 selectively upregulates Duox2 and DuoxA2 protein expression levels that were repressed by IFN-γ treatment (18).

Autoimmune thyroid diseases (AITD) are the most frequent organ-specific autoimmune disturbances, and affect between 3% and 10% of the world's population (23). Hashimoto's thyroiditis (HT) and Graves' disease (GD) are two extreme manifestations of AITD that cause hypothyroidism and hyperthyroidism, respectively. HT is characterized by cytotoxic destruction of the thyroid gland with autoantibodies against TPO and Tg. Stimulating antibodies directed against the TSH receptor (TSAb) are responsible for the hyperthyroid phenotype of GD. Reactive oxygen species (ROS)-mediated oxidative stress could also participate in the pathophysiology of AITD (24–26). Moreover, antioxidant supplementation (selenium or N-acetylcysteine) in combination with antithyroid drugs, especially methimazole, can reduce the severity of AITD symptoms (27,28). The exact source of ROS has not been clearly identified, but they could arise from either the infiltrated leukocytes and/or the thyrocytes themselves. *In vitro* studies using thyroid cell lines to assess how cytokines secreted during the inflammation process affect thyroid function demonstrated repression of Nis, TPO, and Tg expression following cytokine stimulation (IL-1α, IL-1β, IL-6, TGF-β, TNF-α, TNF-β, and IFN-γ) (29). Transgenic mouse models expressing IFN-γ, IL-12, or TGF-β have also been generated to understand the effect of these cytokines better on thyroid pathophysiology (30–32). The role of IL-4 during the inflammatory process has been extensively studied using murine models for experimental autoimmune thyroid disease (EATD). However, the effect of IL-4 in GD pathophysiology remains unclear mainly because none of the EATD models can recapitulate all the hallmarks of the human disease (33–35). Moreover, the direct effects mediated by IL-4 on thyroid physiology remain largely unknown.

Given the IL-4-mediated induction of *DUOX/DUOXA* gene expression and the relative absence of *in vivo* data concerning the potential impact of IL-4 on thyroid function, a new transgenic mouse model was generated that specifically expresses IL-4 in the thyrocytes. These transgenic mice had serum levels of T4 and TSH within the reference ranges, despite an iodide uptake defect and a lower thyroid hormone content. The follicular structure of these mice showed enlarged follicles with thyroid cells containing multiple colloid droplets, suggesting that the gland adapted in order to maintain sufficient thyroid hormone secretion. For the first time, *in vivo* upregulation of pendrin expression is also demonstrated, as well as *Duox1* and *Duoxa1* genes following transgenic overexpression of IL-4.

Materials and Methods

Generation of Thyr-IL-4 transgenic mice

The *mIL-4* cDNA (NM_021283.2) was subcloned into the pIRES2-AcGFP1 vector (Clontech Laboratories) between the *Eco*RI and *Bam*HI sites. The polymerase chain reaction (PCR) amplified fragment containing the mIL-4-IRES2-AcGFP1-SV40PolyA sequence was then cloned between the *Eco*RI and *Xho*I sites of the bTg-βGlobin intron-pBluescript SK+ vector downstream of the bovine thyroglobulin promoter (bTg) (36). The final transgene fragment including the bTg-βGlobin intron-mIL-4-IRES2-AcGFP1-SV40PolyA was excised from the vector by *Sst*II-*Xho*I digestion, and the fragment was gel purified (QIAquick gel extraction kit; Qiagen), followed by a second purification step (QIAquick PCR purification; Qiagen). The transgene cassette was injected at the Université Catholique de Louvain (UCL; Prof. P. Jacquemin) Transgenesis Platform into the pronuclei of B6D2F2 zygotes as previously described (37). Transgenic animals were maintained by mating hemizygous founder animals to wild-type (WT) C57BL/6J mice in a conventional animal housing facility. All transgenic and WT animals used in this study were between 3 and 12 months of age and were from at least the F4 progeny. All animal experiments were approved by the University's ethical committee (CEBEA permit 505N).

The transgene copy number was determined from tail genomic DNA by real-time quantitative PCR (RT-qPCR) amplification using primers directed to the GFP transgenic sequence and the *β-actin* gene for DNA normalization (Supplementary Table S1; Supplementary Data are available online at www.liebertpub.com/thy; $n = 6$ mice) (38). Six pg of DNA was considered to be equivalent to one C57BL/6J mouse cell (39).

RNA extraction and RT-qPCR

Total RNA was extracted from thyroid tissues using the RNeasy kit (Qiagen) and reverse transcribed with random primer hexamers (Roche Applied Science) and the Superscript II reverse-transcriptase (Life Technologies) as described previously (18). RT-qPCR was performed on a 7500 fast RT-qPCR system using Power SYBR Green mix (Life Technologies) with gene-specific, intron spanning primers (Supplementary Table S1). Amplicon purity and identity were assessed by dissociation curve analysis and sequencing of the

PCR products on an automated ABI Prism 3100 sequencer (Life Technologies). Two reference genes (*Retention in Endoplasmic Reticulum 1 homolog* [*Rer1*]) and *TATA box Binding Protein* [*Tbp*]) (40) were used to analyze relative RNA expression with the Pfaffl method (41).

RNA sequencing

Thyroid RNA samples were collected and pooled from three four-month-old transgenic mice (lines 30 and 52) as well as their WT littermates. Indexed cDNA libraries were obtained using the TruSeq Stranded mRNA preparation kit (Illumina) following the manufacturer's recommendations. The multiplexed libraries (9.5 pM) were loaded on a Rapid flow cell. Sequences were produced using a TruSeq Rapid PE cluster and SBS-kit (200 cycles) on a HiSeq 1500 (Illumina). Approximately 44.2, 41.6, 48.3, and 49.1 million paired-end reads corresponded, respectively, to WT lines 30 and 52 and transgenic lines 30 and 52. These reads were mapped against the mouse reference genome (GRCm38.p4/mm10) using STAR software (https://github.com/alexdobin/STAR/releases) to generate read alignments for each sample. Annotated Mus_musculus.GRCm38.79.gtf were obtained from ftp.Ensembl.org. After transcript assembly, gene level counts were obtained using HTSeq (www-huber.embl.de/HTSeq). EdgeR (https://bioconductor.org/packages/edgeR) was used to calculate the level of differential gene expression with biological and data replications with false discovery rate (FDR) values of <0.05 being selected. Genes that showed more than a twofold change in expression between WT and transgenic conditions was considered as being significantly regulated.

Protein isolation and immunodetection

Proteins were extracted in lysis buffer composed of 1% Nonidet P-40 (NP40), 0.05 M of Tris-HCl pH 8, 0.15 M of NaCl, and supplemented with the protease inhibitors Pefabloc (300 ng/mL; Stago BNL), leupetin (5 μg/mL; Molekula), and pepstatin (1 μg/mL), as well as a cOmplete tablet (Roche Applied Science). For thyroid tissues, the samples were first homogenized in the lysis buffer with a rotor stator using a PTFE pestle and glass tube before vortexing for 1 h at 4°C and centrifugation at 10,000 *g* for 10 min. The soluble protein fraction was quantified by a Pierce 660 nm Protein Assay (Thermo Fisher Scientific). Proteins (30 μg) were denatured in Laemmli buffer at 100°C for 1 min, separated on sodium dodecyl sulfate polyacrylamide gel electrophoresis, and transferred to a polyvinylidene difluoride membrane (Immobilon-FL, Millipore). After blocking for 2 h in Odyssey Blocking Buffer (LICOR, Biosciences), the membrane was incubated overnight at 4°C with an anti-GFP primary antibody (1:1000; Clontech). A fluorescent secondary antibody (1:10,000; IRDye800 from LI-COR) was used for image acquisition and quantification with the Odyssey infrared imaging system (LI-COR).

T4, TSH, and IL-4 measurements

Total T4 in 25 μL of serum was measured using a solid-phase ^{125}I radioimmunoassay (RIA; Coat-a-Count T_4, Siemens). TSH serum concentrations were evaluated with a TSH activity bioassay using stable JP26 CHO cells expressing the TSH receptor (42) as described previously (43). Results are expressed as pmol cAMP/50,000 cells. IL-4 quantification was performed by enzyme-linked immunosorbent assay (ELISA; BD OptEIA) on proteins from thyroid tissues, and from the medium of WT and transgenic thyrocytes cultured for 48 h.

Mouse thyroid primary cultures

Samples from between 8 and 10 C57BL/6 mice aged 6–12 months were pooled and used in each culture. Thyroid glands were removed, and the follicles were isolated by collagenase/dispase digestion followed by differential centrifugation (44). The follicles were cultured for 3 days in modified Ham's F-12 medium supplemented with 2.5 μg/mL of fungizone, 100 IU/mL of penicillin, 100 μg/mL of streptomycin (Life Technologies), 5 μg/mL of human apotransferrin, and 1 μg/mL of insulin (Sigma-Aldrich).

Immunohistochemistry

Thyroid lobes were fixed in buffered formalin, embedded in paraffin, sectioned (5 μm), mounted on glass slides, deparaffinized, and rehydrated. For histological analysis, sections were stained with hematoxylin and eosin (H&E) following a routine protocol. For Duox and GFP detection, thyroid tissues were embedded and frozen in Tissue-Tek OCT compound (Sakura). Frozen sections were fixed in acetone for Duox staining. Staining conditions are summarized in Supplementary Table S2. For negative controls, either no antibodies were used or pre-immune serum was substituted (Duox staining). Semi-thin sections and Toluidine Blue coloration were performed as previously described (45). Cyclin D1 positive cells among 1000 cells were counted, and the proliferation index was represented as the mean ± standard error of the mean (SEM; $n = 3$–5 mice). The anti-pendrin antibody (PDS 75-03) was generated by the group of Prof. D. Eladari (Université Paris-Descartes, France) (46). The anti-Duox antibody was generated in the laboratory (5).

Hydrogen peroxide measurements

Hydrogen peroxide accumulated in Krebs-Ringer Hepes (KRH) medium was quantified using a fluorimetric assay based on H_2O_2-dependent oxidation of 440 μM of homovanillic acid (3-methoxy-4-hydroxyphenylacetic acid; Sigma-Aldrich) in the presence of 0.1 mg/mL of horseradish peroxidase type II (Sigma-Aldrich) as previously described (14,47). The amount of H_2O_2 accumulated in the KRH medium over 3 h was normalized to the total RNA content of the cells and represented as μM H_2O_2/μg RNA.

Morphometric analysis by image segmentation

Embedded 5 μm sections were deparaffinized, rehydrated, and treated with Tris-EDTA buffer (10 mM of Tris, 1 mM of EDTA, 0.05% Tween 20, pH 9.0) for 40 min at 98°C before hematoxylin staining. For each group, three different thyroid sections separated by at least 50 μm taken from three to four mice were analyzed.

After acquisition using a Zeiss Axioimager Z1 microscope, images were processed to preserve the maximum intensity of the three primary colors (R, G, and B) in one new module called lightness. Each individual layer corresponding to the thyroid follicle lumen was labeled and analyzed to determine its surface and diameter (major axis). The program

was developed by the Laboratory of Image, Signal Processing and Acoustics (ULB) in the Python language with the mahotas tool box (48).

Iodide uptake and iodide organification assays

Iodide uptake experiments were conducted as described previously, with minor modifications for mouse thyroid samples (49). Briefly, two lobes from different mice were pooled and pre-incubated for 30 min in Krebs-Ringer bicarbonate medium supplemented with 8 mM of glucose, 0.5 g/L of bovine serum albumin (BSA), and 100 μM of methimazole to block iodide organification. Thyroids were incubated with 0.1 μM of KI and 1 μCi/mL of radioactive ^{125}I for 1 h at 37°C. The uptake was calculated as the ratio (T/M) of ^{125}I counts/min/100 mg of tissue (T) to the ^{125}I counts/100 μL medium (M) (Wizard^{TM} 1470 Automatic Gamma Counter, Perkin Elmer).

For iodide organification assays, thyroid lobes were pre-incubated for 30 min in KRH medium with 8 mM of glucose and 0.5 g/L of BSA, and transferred to fresh medium supplemented with 1 μM of KI and ^{125}I (1 μCi/mL) for 2 h as described previously (50). Results were calculated as the ratio of the protein bound ^{125}I (PBI) and the total radioactivity incorporated into the thyroid lobes, and were expressed as the percentage of PBI relative to the total thyroidal ^{125}I.

Tg–T3 and Tg–T4 thyroid content in the thyroid gland

Thyroid lobes were dissected and weighed. Tg–T3 and Tg–T4 contents, corresponding to T3 and T4 associated with Tg, were measured following a previously described protocol (51). The Tg–T3 and Tg–T4 contents were calculated by subtracting the non-Tg-T3/T4, measured without the hydrolysis step, from the total T3 and T4 content.

Statistical analysis

Statistical analysis was performed using an unpaired, two-tailed Student's *t*-test (Prism 5.0, GraphPad Software, Inc.) and the non-parametric Mann–Whitney *U*-test. Data are presented as means ± SEM. Differences were considered significant at $p < 0.05$.

Results

Generation of a Thyr-IL-4 mouse model that overexpresses murine IL-4 *in the thyroid*

Murine IL-4 cDNA was expressed under the control of the bTg promoter that supports thyroid-specific transcription (36). The *mIL-4* sequence was followed by an IRES and GFP-encoding cDNA (Fig. 1A). Five founders were obtained (lines 7, 21, 26, 30, and 52) bearing 6, 1, 12, 2, and 4 copies of the transgene, respectively. ELISA measurement of IL-4 protein levels showed 6- and 12-fold increases in the thyroid tissue from transgenic mouse lines 52 and 30, respectively, relative to WT littermates (Fig. 1B). The mice derived from the other founders showed no significant IL-4 overexpression as illustrated by line 7 mice (Fig. 1B and Supplementary Fig. S1A). *IL-4* and *GFP* transcription in thyroid tissue was quantified by RT-qPCR (Supplementary Fig. S1A). GFP protein expression was also validated in transgenic thyroid tissues by immunoblotting and immunofluorescence (Supplementary Fig. S1B and C). IL-4 secretion was then estimated from primary cultures of WT and Thyr-IL-4 mice. After 48 h of culture, IL-4 accumulated in the culture medium of Thyr-IL-4 thyrocytes to a level of 65 pg/mL/μg of RNA, while only 3 pg/mL/μg of RNA was present in the medium of WT thyrocytes (Fig. 1C). No significant amount of IL-4 could be detected in the mouse sera, suggesting that IL-4 expression was confined to the thyroid gland and did not reach systemic circulation. In addition, there was no significant *Il-4* mRNA overexpression in other major organs that were tested, including the lung, liver, heart, kidney, spleen, testis, and brain (data not shown). IL-4 transgenic animals were viable and reached adulthood without any growth retardation or fertility defect.

Thyroid function is not strongly modified in transgenic Thyr-IL-4 mice

The thyroid status of 3- to 12-month-old mice was examined by measuring the serum levels of total T4 and bioactive TSH. Relative to WT littermates, adult Thyr-IL-4 mice from line 30 showed a slight decrease in T4 level, but the T4 amount was still within the reference range. No significant difference from WT littermates was observed for line 52

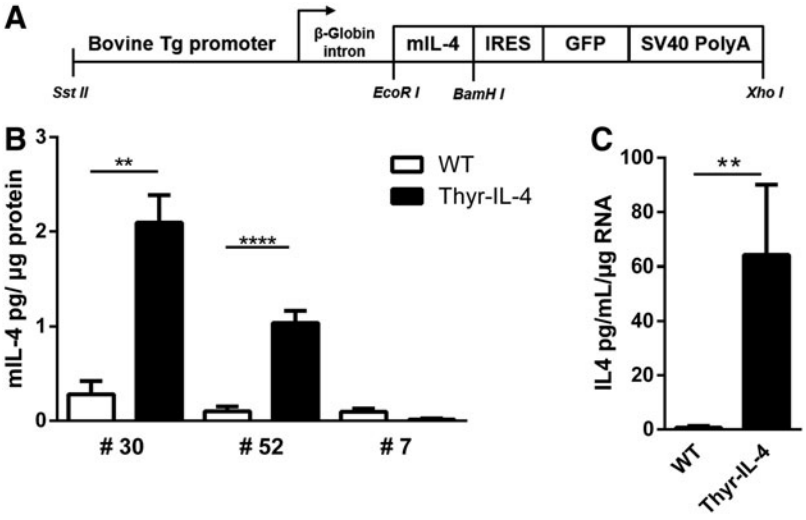

FIG. 1. Generation and characterization of Thyr-IL-4 mice. (**A**) Schematic representation of the Thyr-IL-4 transgenic construct (IRES, internal ribosome entry site; Tg, thyroglobulin). (**B**) Thyroid expression of mIL-4. mIL-4 protein levels were measured by enzyme-linked immunosorbent assay of total protein extracts from wild type (WT) and transgenic thyroid tissues. Protein concentrations were normalized to the total protein content (30 μg; $n \geq 4$ mice). (**C**) mIL-4 secretion by Thyr-IL-4 primo-cultured thyrocytes. Culture medium was collected 48 h after cell seeding. Inteleukin-4 (IL-4) concentration was normalized to the total RNA content of the cells ($n = 4$). Data are presented as means ± standard error of the mean (SEM).

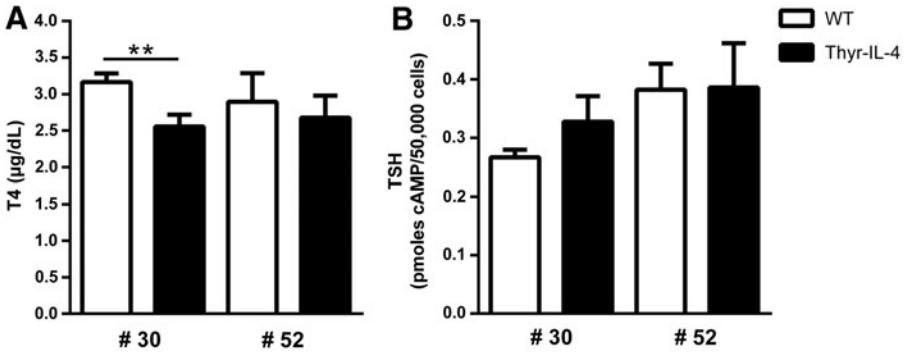

FIG. 2. Thyroid status of adult (3- to 12-month-old) transgenic IL-4 mice. (**A**) Serum total thyroxine (T4) was measured by radioimmunoassay (μg/dL; $n \geq 6$). (**B**) Serum thyrotropin levels were evaluated by bioassay and presented as pmol cAMP produced by 50,000 TSHr-expressing cells ($n \geq 18$). Data are presented as means ± SEM.

(Fig. 2A). Meanwhile, serum TSH showed no statistically significant difference between WT and the two transgenic mouse lines (Fig. 2B).

Transgenic animals show altered thyroid follicular structure with enlarged follicles

The mean weight of thyroids from 10-month-old mice was 3.34 ± 0.79 mg for transgenic lines ($n = 20$) and 3.02 ± 0.82 mg for WT littermates ($n = 28$). Macroscopic evaluations revealed no visible goiter, although a superficially nodular appearance was detected in Thyr-IL-4 mice, particularly from the age of 10 months. This nodularity was likely the consequence of large peripheral follicles that were full of colloid that could be observed upon histological examination (Fig. 3A). The histological architecture of thyroid lobes from 4- and 10-month-old animals was also explored by H&E staining. The most relevant phenotype in the transgenic mice was the increased follicle size seen in a significant proportion of the follicle population in elderly animals. In these enlarged follicles, the thyrocyte

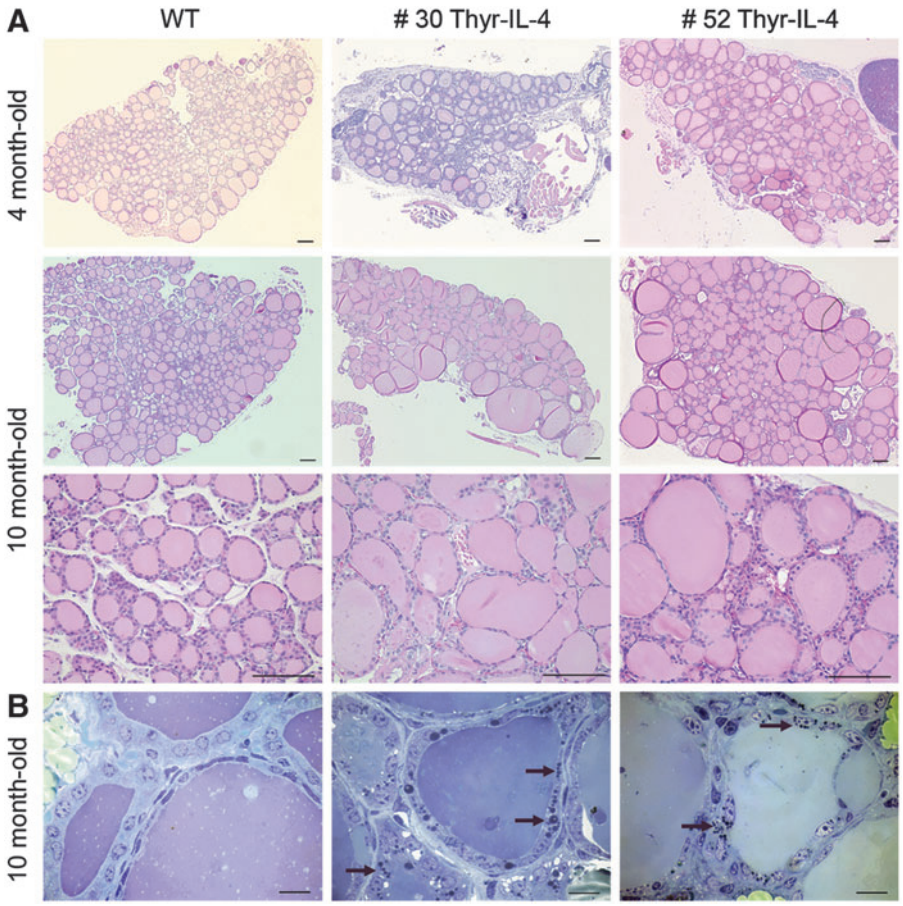

FIG. 3. Enlarged thyroid follicles without goiter in Thyr-IL-4 mice. (**A**) Hematoxylin and eosin staining of thyroid sections (5 μm thick) from 4- and 10-month-old mice. Scale bars: 100 μm. (**B**) Toluidine Blue staining on thyroid semi-thin sections (0.5 μm thick) from 10-month-old animals. Scale bars: 10 μm. Arrows indicate endocytic vesicles. (**C**) Follicle diameter (major axis) distribution in 4- and 10-month-old Thyr-IL-4 and WT animals ($n = 12$ thyroid sections from three mice per genotype) expressed as number of follicles per 100 follicles. (**D**) Mean follicle area in 4- and 10-month-old Thyr-IL-4 and WT mice ($n = 9$–12 thyroid sections per genotype). Data are presented as means ± SEM.

(Continued)

shape was elongated with flattened nuclei usually found in hypoactive follicles. A small proportion of follicles presented with cuboidal cells with cytoplasm extensions and a reduced colloidal lumen. No significant increase in leukocyte infiltration could be detected in transgenic mice compared to WT mice either by H&E or anti-CD45 staining (data not shown). Transgene positive lines without IL-4 overexpression did not show these histological alterations, which supports the conclusion that the observed phenotype is IL-4 dependent. Toluidine Blue staining of semi-thin sections of 10-month-old Thyr-IL-4 thyroid tissues showed numerous endocytic vesicles represented by dark blue spots in enlarged follicles with flat or cuboidal cells that were absent in WT thyroids (Fig. 3B).

To quantify these structural differences, morphometric analyses were conducted by measuring the follicular diameter (major axis) and the area of 7425 WT and 8060 Thyr-IL-4 follicles. Figure 3C shows the data concerning the follicular diameter presented as frequency per hundred follicles. Most

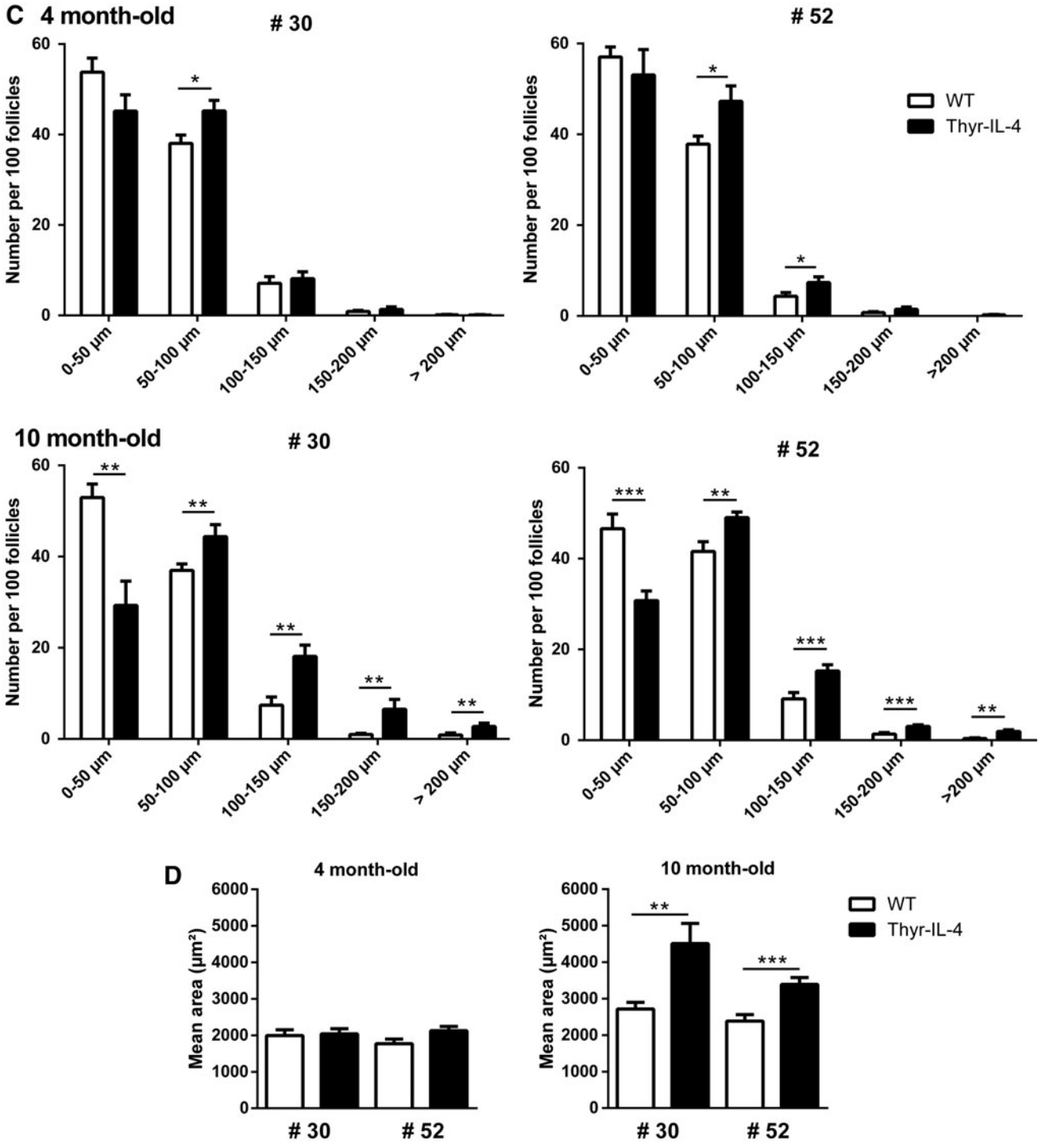

FIG. 3. (*Continued*)

follicles from WT mice had a diameter <100 μm (93 ± 1% at 4 months and 90 ± 2% at 10 months). At four months, a small but significant proportion of follicles with a diameter between 50 and 100 μm was present in Thyr-IL-4 tissues (45 ± 2% vs. 38 ± 2% for line 30 and 47 ± 3% vs. 37 ± 2% for line 52). By 10 months of age, transgenic follicles showed a significantly increased proportion of enlarged follicles with a diameter >100 μm (28 ± 5% vs. 9 ± 2% for line 30 and 20 ± 2% vs. 10 ± 2% for line 52). The mean follicle area in 10-month-old Thyr-IL-4 animals was also increased relative to WT littermates (4508 ± 557 μm^2 vs. 2714 ± 184 μm^2 for line 30 and 3393 ± 178 μm^2 vs. 2383 ± 185 μm^2 for line 52; Fig. 3D).

Gene profiling of Thyr-IL-4 thyroids reveals modulated expression of genes involved in thyroid function

Whole transcriptome sequencing was performed on thyroids of four-month-old animals. A total of 15,068 transcripts expressed in either WT or transgenic thyroids were identified. Genes showing a more than a twofold change from WT animals with a significant FDR (<0.05) were used to discriminate differentially expressed genes. Together, thyroids from transgenic lines 30 and 52 had 583 up- and 203 downregulated genes compared with their WT littermates (Supplementary Table S3). Pathway analysis of these differentially regulated genes using DAVID software (52,53) revealed involvement of several signaling pathways with 12 implicated in immunity, including one thought to be involved in AITD (Supplementary Table S4). The thyroid overexpression of the IL-4 transgene was confirmed by an 18-fold increase in expression seen in transgenic thyroids. Thyroid expression of the type II IL-4 receptor was confirmed by multiple reads corresponding to *Il-4rα* and *Il-13rα1* genes measured in WT and transgenic tissues (54). Supplementary Table S5 shows a list of genes that are described in the literature to be regulated by the IL-4 pathway (55–58) and that were significantly modulated in Thyr-IL-4 thyroids. RT-qPCR experiments confirmed the modulated expression of *Il-13rα2*, a decoy IL-13 receptor, and *Il-4rα* transcripts (Fig. 4A). These data strongly suggest that mIL-4 was not only highly expressed in the thyroid, but also exerted a functional effect.

Among genes related to thyroid function, including *Tshr*, *Tpo*, *Iyd* (iodotyrosine deiodinase), *Duox1*, *Duoxa1*,

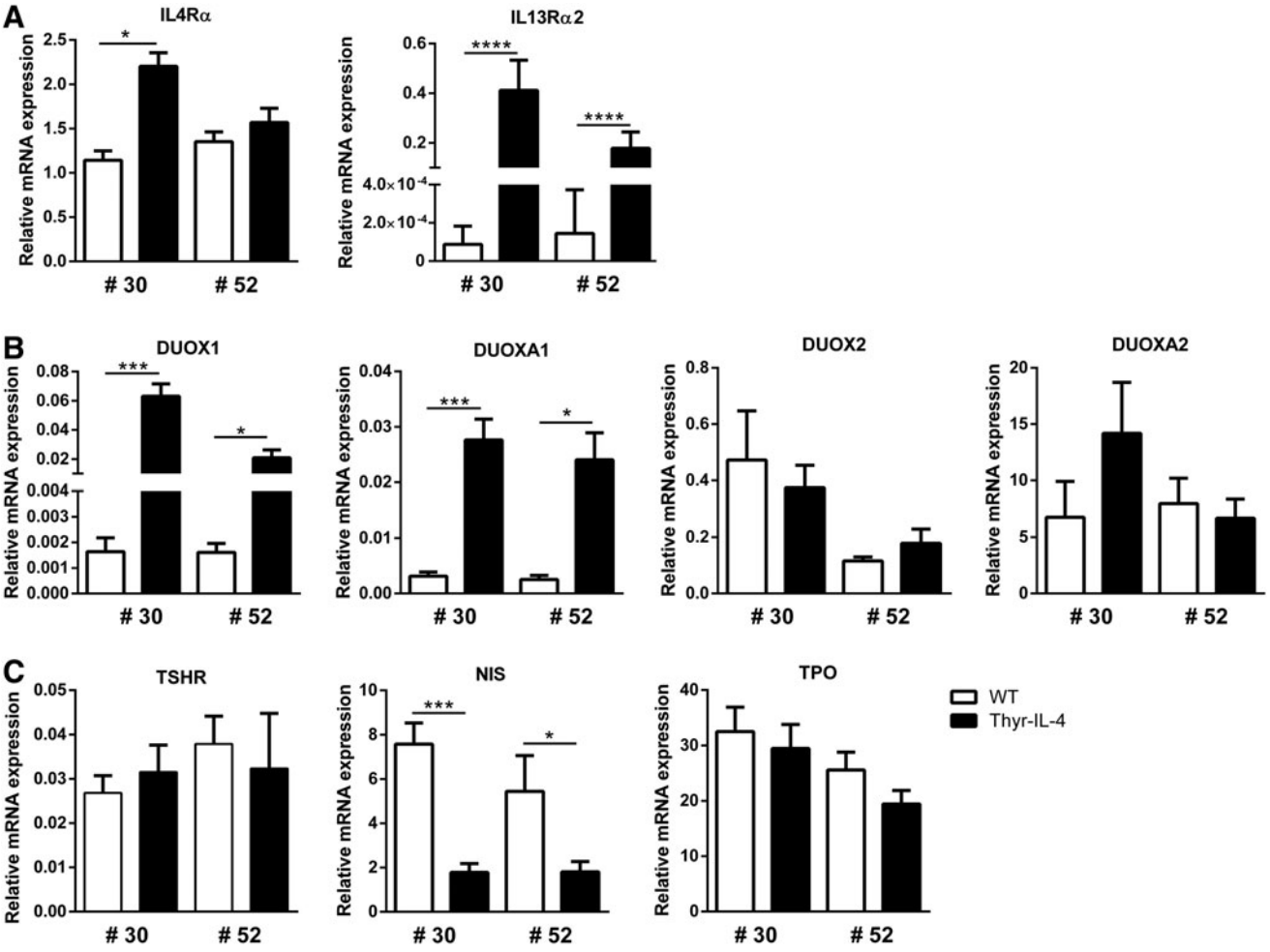

FIG. 4. Aberrant thyroid IL-4 overexpression modulates *Nis/Slc5a5*, *Duox1*, and *Duoxa1* gene expression in adult (3- to 12-month-old) transgenic mice. (**A**) mRNA expression of *Il-4rα*, and *Il-13rα2* measured by quantitative reverse transcription polymerase chain reaction (RT-qPCR) of WT and Thyr-IL-4 thyroid tissues. Relative mRNA expression was normalized to the reference genes *Rer1* and *Tbp* ($n \geq 6$). (**B**) *Duox1*, *Duox2*, *Duoxa1*, and *Duoxa2* mRNA relative expression ($n \geq 5$). (**C**) Relative mRNA expression of *Tshr*, *Nis/Slc5a5*, and *Tpo* ($n \geq 6$). Data are presented as means ± SEM.

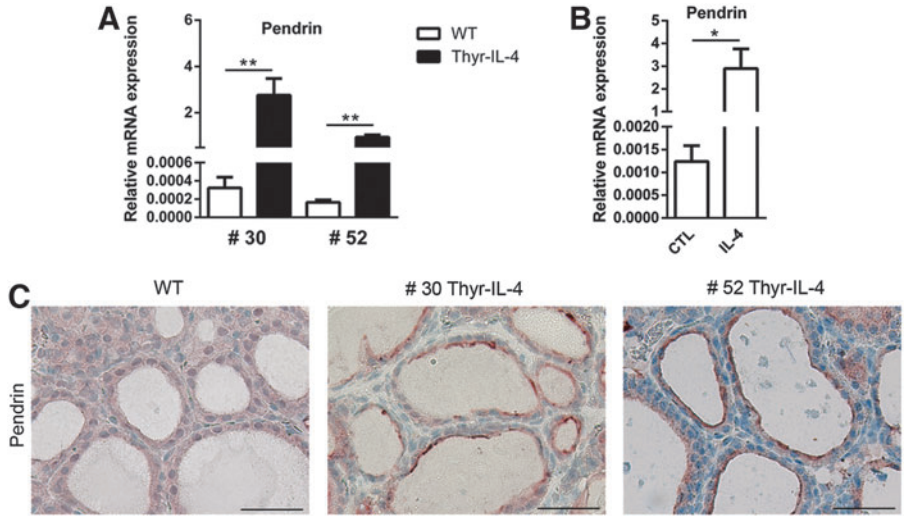

FIG. 5. Pendrin overexpression in thyroids from transgenic animals. (**A**) Relative *Slc26a4* (*pendrin*) mRNA expression measured by RT-qPCR in WT and Thyr-IL-4 thyroid tissue ($n \geq 4$ mice). (**B**) Relative *Slc26a4* mRNA expression in WT thyrocyte primary cultures after 48 h of stimulation with 100 ng/mL of mIL-4 ($n = 4$). (**C**) Thyroid sections (5 μm thick) from WT and transgenic mice were submitted to immunohistochemistry for pendrin expression. Pendrin apical staining was clearly increased in Thyr-IL-4 tissues. Scale bars: 50 μm ($n = 3$). Data are presented as means ± SEM.

Duox2, *Duoxa2*, *Slc26a4* (anion exchanger pendrin), *Ano1* (Anoctamine-1), and *Slc5a5* (*Nis*), the expression of only *Duox1*, *Duoxa1*, *Pendrin*, and *Nis* transcripts was significantly modulated (Supplementary Table S6). Previously, an IL-4-dependent positive modulation of both *Duox1/Duoxa1* and *Duox2/Duoxa2* was demonstrated in primary mouse thyrocyte cultures treated for 48 h with 100 ng/mL of mIL-4 (18). Here, it is shown that expression of mIL-4 in the thyroid *in vivo* selectively upregulates *Duox1* and *Duoxa1* gene expression (Fig. 4B). Interestingly, both *Duox1*/*Duoxa1* and *Duox2*/*Duoxa2* transcripts were upregulated in primary cultures of thyrocytes from Thyr-IL-4 mice compared with WT thyroid cultures (Supplementary Fig. S2). No *Duox*/*Duoxa* gene induction was observed in the IL-4 negative transgenic line 7 (Supplementary Fig. S3). *Nis* expression showed a significant three- to fivefold decrease as confirmed by RT-qPCR (Fig. 4C), while *Tpo* and *Tshr* expression did not differ between Thyr-IL-4 and WT animals.

Surprisingly, the thyroid marker showing the most robust modulation was pendrin, as evidenced by the more than a 1000-fold increase in mRNA levels seen with Thyr-IL-4 lines 30 and 52 relative to WT mice (Fig. 5A). Although a previous study demonstrated that the *Slc26a4* gene encoding pendrin was induced in bronchial epithelium following IL-4 exposure (57), to date no data concerning IL-4-dependent pendrin regulation have been reported for the thyroid. The regulation of pendrin expression was confirmed in WT primary thyrocyte cultures stimulated for 48 h with mIL-4 (100 ng/mL; Fig. 5B). Moreover, pendrin protein staining was also enhanced in transgenic animals, particularly at the follicular apical membrane (Fig. 5C).

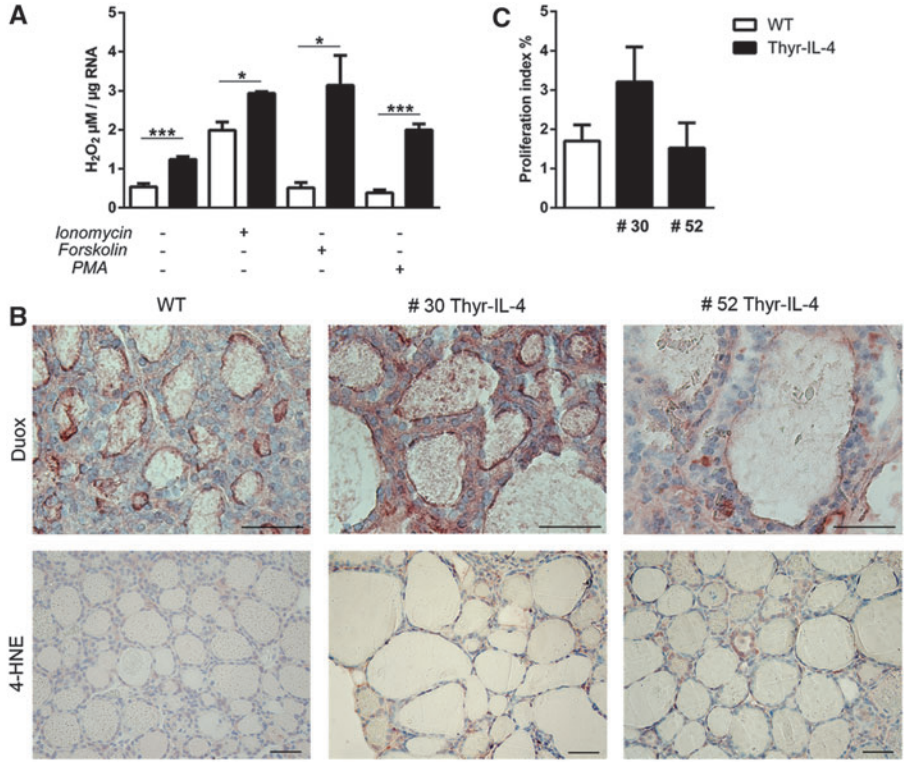

FIG. 6. Consequences of *Duox1*/*Duoxa1* overexpression in Thyr-IL-4 thyroid tissue. (**A**) H_2O_2 production by thyroid tissues. Extracellular H_2O_2 was allowed to accumulate for 3 h in control (–) and stimulated (+) thyrocytes (2 μM of ionomycin, 10 μM of forskolin, or 5 μM of PMA; $n = 3$). H_2O_2 levels were normalized to the total RNA content. (**B**) Duox and 4-HNE immunodetection in thyroid sections (5 μm thick) from 10-month-old WT and transgenic mice. Duox and 4-HNE immunostaining were localized at the apical membrane and in the cytoplasm, respectively. Scale bars: 50 μm ($n = 3$). (**C**) Proliferation index of cyclin D1 staining quantified from thyroid sections ($n \geq 4$ mice). Data are presented as means ± SEM.

Consequences of Duox1 and Duoxa1 upregulation in Thyr-IL-4 thyroid

Duox proteins are Ca^{2+}-dependent NADPH oxidases that produce extracellular H_2O_2, a key step in thyroid hormonogenesis (4). To assess the functional consequences of Duox induction, the amount of extracellular H_2O_2 generated by thyroid tissues from WT and Thyr-IL-4 animals (a mixture of lines 30 and 52) was quantified. Under all conditions (i.e., basal, 2 μM of ionomycin, 10 μM of forskolin, or 5 μM of phorbol 12 myristate 13-acetate [PMA]), H_2O_2 levels were increased in transgenic tissues compared with WT (Fig. 6A). Forskolin alone was sufficient to stimulate H_2O_2 production in Thyr-IL-4 thyroids but not in WT animals. This result strongly suggests that Duox1 contributes to H_2O_2 production by Thyr-IL-4 thyroids. Moreover, upon stimulation with ionomycin and PMA, the H_2O_2 concentration generated from transgenic primary thyrocyte cultures was significantly increased by twofold compared with WT cells (data not shown), and was very similar to the amount of H_2O_2 produced by WT thyrocytes stimulated with exogenous mIL-4 (18).

Analysis of Duox protein expression by immunohistochemistry confirmed the apical membrane localization of these proteins in either small or large follicles. However, because the anti-Duox antibody was not isoform specific, an intensification of Duox staining in transgenic tissues could not be demonstrated (Fig. 6B). Instead, the oxidative stress marker, 4-hydroxy-2-nonenal (4-HNE), revealed heterogeneous staining of the follicles with no significant increase in Thyr-IL-4 mice (Fig. 6B). Moreover, expression of key antioxidant related genes, including *heme oxygenase 1* (*Hmox1*), *glutathione peroxidase 3* (*Gpx3*), *thioredoxin reductase 1* (*Txnrd1*), and *glutamate cysteine ligase* (*Gclm*), was not significantly modulated in four- (whole transcriptome sequencing) and 10-month-old (RT-qPCR, data not shown) Thyr-IL-4 thyroids compared to WT.

To assess whether the enlargement seen in transgenic follicles is due to a higher proliferation rate, cyclin D1 immunostaining was performed. In Thyr-IL-4 thyroids, rare proliferating cells could be observed. Furthermore, the proliferation index was similar between WT and Thyr-IL-4 thyroids, with no particular proliferation capacity of IL-4 expressing thyrocytes seen (Fig. 6C).

Reduction of Nis expression results in impaired iodide uptake and lower thyroid T3 and T4 content

To evaluate the physiological consequences of partial suppression of *Slc5a5* expression in Thyr-IL-4 mice, *ex vivo* iodide uptake experiments were conducted in thyroid lobes. For both transgenic lines 30 and 52, iodide uptake was decreased by threefold relative to WT glands, thus confirming the presence of an iodide transport defect in transgenic animals (Fig. 7A). In all animals tested, iodide uptake (T/M) could be abolished in the presence of $NaClO_4$, which supports a Nis-specific activity.

Next, the T4 synthesis capacity of the enlarged follicles composed of elongated cells with flattened nuclei that were suggestive of hypoactive units was investigated. T4 immunostaining in thyroids of 10-month-old mice showed positive labeling in WT and transgenic animals in small and enlarged follicles with no visible differences (Fig. 7B). The

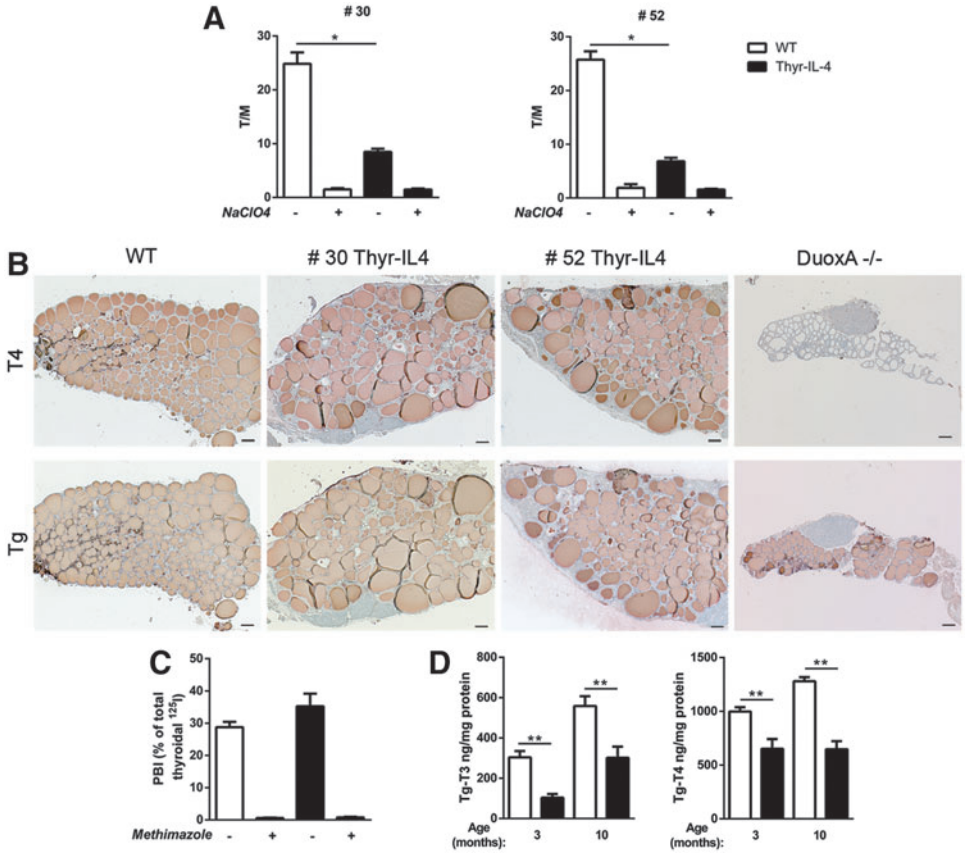

FIG. 7. Iodide uptake is decreased in transgenic mice, but T4 synthesis is maintained. (**A**) ^{125}I uptake measured *ex vivo* on thyroid lobes and expressed as a T/M ratio (see Methods; $n=4$). $NaClO_4$ was used as a control for Nis-dependent iodide transport. (**B**) T4 and Tg immunostaining on serial thyroid sections (5 μm thick) from 10-month-old WT, Thyr-IL-4 mice, and *Duoxa*$^{-/-}$ mice. Scale bars: 100 μm ($n=3$). (**C**) Iodide organification assays performed *ex vivo* on thyroid lobes expressed as protein bound ^{125}I percentage (see Methods; $n=4$). (**D**) Tg–T3 and Tg–T4 content measured in thyroid lobes from young (3- to 4-month-old) and old (10- to 11-month-old) mice ($n \geq 4$). Data are presented as means ± SEM.

Tg content also seemed to be similar between the two genotypes. No positive T4 staining was detected in the negative control, the *Duoxa–/–* mice, which have an iodide organification defect caused by impaired H_2O_2 generation (11). To explore the overall efficiency of the iodination process, the proportion of PBI was measured. Methimazole pretreatment inhibited iodide organification, showing a specific TPO activity. Thyr-IL-4 thyroids presented a similar proportion of PBI as that seen in WT tissues, suggesting no iodide organification defect (Fig. 7C). However, a minor, but not significant, diminution of the total amount of organified iodide per milligram of Thyr-IL-4 tissue could be detected (data not shown). The thyroid content of Tg–T3 and Tg–T4 (T3 and T4 associated with the Tg macromolecule) was quantified (51). Transgenic thyroid tissues contained significantly less Tg–T3 and Tg–T4 relative to WT counterparts either in young (three- to four-month-old) and old (10- to 11-month-old) animals (Fig. 7D).

Discussion

A role for inflammatory cytokines, including IL-4, has been widely documented in inflammation in general and suggested in AITD. Here, the *in vivo* pathophysiological consequences of chronic exposure of mouse thyroid glands to the Th2 cytokine IL-4 were investigated using the well-characterized bTg promoter (36). In this new mouse model, it was found that IL-4 expression was restricted to thyroid tissue and functional as evidenced by: (i) IL-4 transgene expression at the mRNA and protein level; (ii) extracellular secretion of IL-4 from Thyr-IL-4 thyroid cells; (iii) GFP localization in follicular cells; and (iv) gene profiling showing modulated expression of multiple genes involved in inflammation.

Recently, Th2 cytokine-mediated induction of *DUOX* and *DUOXA* expression in *in vitro* models of human (*DUOX2*/*DUOXA2*) and mouse (*Duox1*/*Duoxa1* and *Duox2*/*Duoxa2*) thyrocytes was demonstrated. Here, positive regulation of only *Duox1* and *Duoxa1* genes *in vivo* in Thyr-IL-4 mice was clearly identified. However, primary cultures of transgenic thyrocytes recapitulated the increased expression of both *Duox1*/*Duoxa1* and *Duox2/Duoxa2* isoforms compared with WT cells. The apparent inconsistency between tissue and cell culture most likely resulted from cellular de-differentiation during the culture, as suggested by the strong downregulation of *Duox2/Duoxa2* (Fig. 4B and Supplementary Fig. S2), *Tpo*, and *Slc5a5* mRNA expression (data not shown). No significant increase in *Ifn-γ* expression was detected by RNA sequencing in Thyr-IL-4 thyroids, which could also explain the repression of *Duox2* expression in thyroid tissue. A similar repression of these differentiation genes was previously reported in human thyroid cancer cell lines (59). Together, these results show the limitations that can be associated with experiments performed with thyrocyte cultures or cell lines as thyroid physiological models. Moreover, induction of *DUOX1* expression via the IL-13 pathway was recently demonstrated in both human primary thyrocytes and the thyroid cell line Hthy-ori3.1 (60). These data clearly indicate that IL-4 or IL-13-dependent induction of *DUOX* gene transcription is species- and cell type-dependent and can be markedly influenced by the differentiation status of the cell.

In the human thyroid, the *DUOX2* mRNA content is two- to fivefold higher than *DUOX1* (61). Thyroid mouse RNA profiling in this study also showed an increased *Duox2*/*Duox1* ratio (Supplementary Table S6), suggesting that the Duox2 isoform is also a major component of the murine thyroid H_2O_2-generating system. However, *Duox2*/*Duox1* expression levels were very low relative to other thyroid function markers such as *Tpo* and iodotyrosine deiodinase (*Iyd*), which were the most abundant transcripts after *Tg* mRNA (Supplementary Table S6). In Thyr-IL-4 thyroids, despite the *Duox1* overexpression, *Duox2* remained the major Duox isoform. This could explain the absence of a significant increase in the oxidative stress marker 4-HNE in the Thyr-IL-4 transgenic mice.

The *Slc26a4* gene encodes the transmembrane protein anion exchanger pendrin that exchanges chloride for bicarbonate, iodide, and thiocyanate (SCN^-) (62). The pendrin protein is expressed not only in the thyroid, but also in many other tissues, including the kidney, the airways, the mammary gland, and the inner ear (63). The role of pendrin in thyroid apical iodide transport is still a matter of debate. Pendred syndrome, an autosomal recessive disorder, is mainly characterized by deafness, but some patients also present with hypothyroidism (63). No thyroid phenotype has been reported for *Slc26a4* KO mice (64), suggesting that pendrin plays a non-essential role in iodide transport, at least in the mouse, and that alternate transporters, most likely the Ca^{2+}-activated ion channel Anoctamin-1, can mediate apical iodide efflux (1,2). Using Thyr-IL-4 transgenic mice, this study showed for the first time an IL-4-dependent induction of *Slc26a4* transcription, which was associated with increased apical expression of pendrin. TSH can rapidly stimulate pendrin membrane translocation via the PKA pathway (65), although the Thyr-IL-4 mice showed no significant increase in serum TSH level relative to WT mice (Fig. 2B). The IL-4-mediated pendrin expression observed here suggests that pendrin may have a role in thyroid physiology during inflammation. This possibility is consistent with a previous study in bronchial epithelial cells showing that IL-4/IL-13-mediated *SLC26A4* induction via direct promoter transactivation by the JAK1-STAT6 pathway (66,67) is associated with increased SCN^- apical transport (57). In the presence of H_2O_2 produced by Duox, SCN^- is oxidized in the microbicide compound hypothyocyanite ($OSCN^-$) by mucosal lactoperoxidase, which plays an important role in innate immunity (68,69).

Although Thyr-IL-4 mice show neither growth retardation nor hypothyroidism, a clear repression of *Nis* expression associated with impaired iodide uptake (reduced T/M) was seen. This result suggests that an increase in Duox1-mediated ROS could inactivate Nis function in Thyr-IL-4 mice to inhibit iodide uptake further (70). In Thyr-IL-4 thyroid tissue, iodide organification was not compromised (as shown by a similar PBI), but the thyroid content of T3 and T4 bound to Tg was significantly reduced. Moreover, the lack of significant induction of iodotyrosine dehalogenase, which is involved in iodide recycling, suggests that this dehalogenase does not contribute to the maintenance of the normal serum T4 levels in these transgenic animals (71). The most striking phenotype observed in Thyr-IL-4 thyroid tissue was the increased proportion of enlarged follicles in old mice. Despite their hypofunctional aspects (e.g., elongated cells with flattened nuclei), these enlarged follicles still stained positive

for T4. This phenotype is most likely the result of specific biological effects of IL-4 because its severity was related to the level of IL-4 expression in the thyroid gland, which was higher in transgenic line 30 than in line 52, and not detected in line 7. Numerous intracellular dense bodies were present in the cytoplasm of Thyr-IL-4 thyrocytes. These colloid droplets could reflect an intense endocytosis of luminal Tg to maintain normal levels of thyroid hormone secretion despite decreased amounts of iodinated Tg contained in the gland (lower Tg–T3 and Tg–T4) (72). However, the exact molecular mechanism behind this IL-4 mediated phenotype is unclear and awaits further characterization in future studies.

Overexpression of the anion exchanger pendrin could partially compensate for the lower basal Nis-dependent iodide uptake by facilitating the apical efflux of iodide. Pendrin may also be implicated in the alkalinization of the follicular lumen by exchanging Cl^- for HCO_3^- to promote generation of follicular H_2O_2 (50,73,74). However, no significant increase in iodide organification was seen in transgenic thyroid tissues. A thyroid mouse model with overexpression of the proto-oncogene pituitary tumor transforming gene-binding factor also showed modified thyroid architecture that featured enlarged follicles (75), but this phenotype, which was associated with hyperproliferative lesions, was not observed in Thyr-IL-4 mice. As such, the follicular volume may have resulted from a bidirectional transepithelial transport of basal to apical Cl^- and an opposite Na^+ flux (76). IL-4 and IL-13 have been reported to modulate these Na^+Cl^- currents in certain cell types by regulating the expression of channels and transporters, including aquaporins (62). However, pendrin overexpression would favor the reduction of the colloid space by promoting reabsorption of luminal chloride. As such, a cross of Thyr-IL-4 mice with *Slc26a4* KO animals (64) would likely provide valuable information about the contribution of pendrin to the Thyr-IL-4 phenotype.

The common simplified view that separates HT and GD on the basis of the Th1 and Th2 inflammatory response, respectively, was recently reviewed (77). RT-qPCR performed on GD and HT thyroid tissue samples showed an increase in IL-4 transcripts in GD compared with HT thyroids, but also augmented IFN-γ expression in GD compared with control patients (78). An *IL-4* gene haplotype is associated with pediatric GD, and more recent plasma analysis of a GD cohort demonstrated increased IL-4 protein levels in recurrent GD patients (79,80). However, data obtained from various EATD murine models were even more complex. *Il-4*$^{-/-}$ BALB/c mice immunized with TSHr-expressing cells are resistant to GD development and showed a delayed antibody response (34). Meanwhile, another model involving immunization of BALB/c mice with TSHr-expressing adenovirus showed that coinjection of an adenovirus expressing IL-4 significantly reduced TSAb levels and incidence of hyperthyroidism (35). No significant increase in leukocyte infiltration could be detected in Thyr-IL-4 thyroid glands, which was likely due to the absence of immunization experiments and also to the genetic background of the mice (C57BL/6J) that are known to be EATD resistant (81). However, differential expression of multiple genes involved in inflammatory pathways in Thyr-IL-4 thyroid samples was observed (Supplementary Table S3), suggesting that Thyr-IL-4 mice could be used to investigate the role of IL-4 in AITD when appropriate immunization protocols are used after crossing these mice with other AITD permissive mice, such as the recently reported TSHr-transgenic NOD.H2^{h4} mice that spontaneously develop anti-TSHr antibodies (82).

In GD patients, the main source of IL-4 is the thyroid lymphocyte infiltrate, which is generated by the thyrocytes themselves in Thyr-IL-4 mice. The effects associated with uncontrolled ectopic production of IL-4 do not reflect the actual situation in GD patients who present with thyroid inflammation, TSHr-autoantibodies, and thyroid hyperstimulation; the latter would likely compensate for the IL-4-mediated *Nis* repression observed in the transgenic animals in the present study. In contrast, enhanced thyroid apical expression of pendrin was also reported in GD patients (83–86). Moreover, autoantibodies against pendrin have been found in the sera of AITD patients, and *SLC26A4* has been proposed to be a new AITD susceptibility gene (87,88).

In conclusion, the development of a novel mouse model with targeted IL-4 expression in the thyroid is herein described. Characterization of these mice showed that ectopic expression of IL-4 in the thyroid positively regulates *Duox1*, *Duoxa1*, and *Slc26a4* expression while inhibiting *Slc5a5* expression. The Thyr-IL-4 mice had impaired thyroid iodide uptake, increased follicular size, and lower thyroidal T3 and T4 content, but serum levels of T4 and TSH were within reference ranges. No leukocyte infiltration was clearly established.

Acknowledgments

We gratefully acknowledge Dr. H. Grasberger for the *Duoxa* KO mice, Prof. D. Eladari for the pendrin antibody 75-03, and Prof. P. Jacquemin of the UCL transgenesis platform. We thank Dr. B. Contempré and Prof. R. Beauwens for their interest in this work and their advice. We thank J.M. Vanderwinden for the use of the microscope facility. We extend special thanks to C. Degraef, B. Bournonville, C. Massart, M. de Bournonville, and C. de Ville de Goyet for their excellent technical assistance, and to F. Libert and A. Lefort for RNA sequencing. This work was supported by the Fonds de la Recherche Scientifique (FRS-FNRS), the Fund Doctor J.P. Naets, managed by the King Baudouin Foundation, the Fondation Rose et Jean Hoguet, the Fonds Lekime-Ropsy, and grant DK15070 from the U.S. National Institutes of Health to S.R. Z.E. is a recipient of a fellowship from the Fonds pour la Formation à la Recherche dans l'Industrie et l'Agriculture.

Author Disclosure Statement

No competing financial interests exist.

References

1. Twyffels L, Strickaert A, Virreira M, Massart C, Van Sande J, Wauquier C, Beauwens R, Dumont JE, Galietta LJ, Boom A, Kruys V 2014 Anoctamin-1/TMEM16A is the major apical iodide channel of the thyrocyte. AJP Cell Physiol **307:**1102–1112.
2. Iosco C, Cosentino C, Sirna L, Romano R, Cursano S, Mongia A, Pompeo G, di Bernardo J, Ceccarelli C, Tallini G, Rhoden KJ 2014 Anoctamin 1 is apically expressed on thyroid follicular cells and contributes to ATP- and calcium-activated iodide efflux. Cell Physiol Biochem **34:** 966–980.

3. Silveira JC, Kopp PA 2015 Pendrin and anoctamin as mediators of apical iodide efflux in thyroid cells. Curr Opin Endocrinol Diabetes Obes **22:**374–380.
4. Song Y, Driessens N, Costa M, De Deken X, Detours V, Corvilain B, Maenhaut C, Miot F, Van Sande J, Many MC, Dumont JE 2007 Roles of hydrogen peroxide in thyroid physiology and disease. J Clin Endocrinol Metab **92:**3764–3773.
5. De Deken X, Wang D, Many MC, Costagliola S, Libert F, Vassart G, Dumont JE, Miot F 2000 Cloning of two human thyroid cDNAs encoding new members of the NADPH oxidase family. J Biol Chem **275:**23227–23233.
6. Dupuy C, Ohayon R, Valent A, Noël-Hudson MS, Dème D, Virion A 1999 Purification of a novel flavoprotein involved in the thyroid NADPH oxidase. J Biol Chem **274:**37265–37269.
7. Grasberger H, Refetoff S 2006 Identification of the maturation factor for dual oxidase. Evolution of an eukaryotic operon equivalent. J Biol Chem **281:**18269–18272.
8. Rigutto S, Hoste C, Grasberger H, Milenkovic M, Communi D, Dumont JE, Corvilain B, Miot F, De Deken X 2009 Activation of dual oxidases Duox1 and Duox2: differential regulation mediated by cAMP-dependent protein kinase and protein kinase C-dependent phosphorylation. J Biol Chem **284:**6725–6734.
9. Johnson KR, Marden CC, Ward-Bailey P, Gagnon LH, Bronson RT, Donahue LR 2007 Congenital hypothyroidism, dwarfism, and hearing impairment caused by a missense mutation in the mouse dual oxidase 2 gene, *Duox2*. Mol Endocrinol **21:**1593–1602.
10. Donkó Á, Ruisanchez É, Orient A, Enyedi B, Kapui R, Péterfi Z, De Deken X, Benyó Z, Geiszt M 2010 Urothelial cells produce hydrogen peroxide through the activation of Duox1. Free Radic Biol Med **49:**2040–2048.
11. Grasberger H, De Deken X, Mayo OB, Raad H, Weiss M, Liao XH, Refetoff S 2012 Mice deficient in dual oxidase maturation factors are severely hypothyroid. Mol Endocrinol **26:**481–492.
12. Moreno JC, Bikker H, Kempers MJE, van Trotsenburg AS, Baas F, de Vijlder JJM, Vulsma T, Ris-Stalpers C 2002 Inactivating mutations in the gene for thyroid oxidase 2 (*THOX2*) and congenital hypothyroidism. N Engl J Med **347:**95–102.
13. Grasberger H 2010 Defects of thyroidal hydrogen peroxide generation in congenital hypothyroidism. Mol Cell Endocrinol **322:**99–106.
14. Milenkovic M, De Deken X, Jin L, De Felice M, Di Lauro R, Dumont JE, Corvilain B, Miot F 2007 Duox expression and related H_2O_2 measurement in mouse thyroid: onset in embryonic development and regulation by TSH in adult. J Endocrinol **192:**615–626.
15. Opitz R, Maquet E, Zoenen M, Dadhich R, Costagliola S 2011 TSH receptor function is required for normal thyroid differentiation in zebrafish. Mol Endocrinol **25:**1579–1599.
16. D'Andrea B, Iacone R, Di Palma T, Nitsch R, Baratta MG, Nitsch L, Di Lauro R, Zannini M 2006 Functional inactivation of the transcription factor Pax8 through oligomerization chain reaction. Mol Endocrinol **20:**1810–1824.
17. Christophe-Hobertus C, Lefort A, Libert F, Christophe D 2012 Functional inactivation of thyroid transcription factor-1 in PCCl3 thyroid cells. Mol Cell Endocrinol **358:**36–45.
18. Raad H, Eskalli Z, Corvilain B, Miot F, De Deken X 2013 Thyroid hydrogen peroxide production is enhanced by the Th2 cytokines, IL-4 and IL-13, through increased expression of the dual oxidase 2 and its maturation factor DUOXA2. Free Radic Biol Med **56:**216–225.
19. De Deken X, Corvilain B, Dumont JE, Miot F 2014 Roles of DUOX-mediated hydrogen peroxide in metabolism, host defense, and signaling. Antioxid Redox Signal **20:**2776–2793.
20. Harper RW, Xu C, Eiserich JP, Chen Y, Kao CY, Thai P, Setiadi H, Wu R 2005 Differential regulation of dual NADPH oxidases/peroxidases, Duox1 and Duox2, by Th1 and Th2 cytokines in respiratory tract epithelium. FEBS Lett **579:**4911–4917.
21. Hirakawa S, Saito R, Ohara H, Okuyama R, Aiba S 2011 Dual oxidase 1 induced by Th2 cytokines promotes STAT6 phosphorylation via oxidative inactivation of protein tyrosine phosphatase 1B in human epidermal keratinocytes. J Immunol **186:**4762–4770.
22. Wu Y, Antony S, Juhasz A, Lu J, Ge Y, Jiang G, Roy K, Doroshow JH 2011 Up-regulation and sustained activation of Stat1 are essential for interferon-gamma (IFN-gamma)-induced dual oxidase 2 (Duox2) and dual oxidase A2 (DuoxA2) expression in human pancreatic cancer cell lines. J Biol Chem **286:**12245–12256.
23. Rapoport B, McLachlan SM 2001 Thyroid autoimmunity. J Clin Invest **108:**1253–1259.
24. Burek CL, Rose NR 2008 Autoimmune thyroiditis and ROS. Autoimmun Rev **7:**530–537.
25. Zarković M 2012 The role of oxidative stress on the pathogenesis of Graves' disease. J Thyroid Res **2012:**1–5.
26. Marique L, Senou M, Craps J, Delaigle A, Van Regemorter E, Wérion A, Van Regemorter V, Mourad M, Nyssen-Behets C, Lengelé B, Baldeschi L, Boschi A, Brichard S, Daumerie C, Many MC 2015 Oxidative stress and upregulation of antioxidant proteins, including adiponectin, in extraocular muscular cells, orbital adipocytes, and thyrocytes in Graves' disease associated with orbitopathy. Thyroid **25:**1033–1042.
27. Marcocci C, Kahaly GJ, Krassas GE, Bartalena L, Prummel M, Stahl M, Altea MA, Nardi M, Pitz S, Boboridis K, Sivelli P, von Arx G, Mourits MP, Baldeschi L, Bencivelli W, Wiersinga W 2011 Selenium and the course of mild Graves' orbitopathy. N Engl J Med **364:**1920–1931.
28. Poncin S, Colin IM, Decallonne B, Clinckspooor I, Many MC, Denef JF, Gerard AC 2010 N-acetylcysteine and 15 deoxy-Δ12,14-prostaglandin J2 exert a protective effect against autoimmune thyroid destruction *in vivo* but not against interleukin-1α/interferon γ-induced inhibitory effects in thyrocytes *in vitro*. Am J Pathol **177:**219–228.
29. Dohán O, De La Vieja A, Paroder V, Riedel C, Artani M, Reed M, Ginter CS, Carrasco N 2003 The sodium/iodide symporter (NIS): characterization, regulation, and medical significance. Endocr Rev **24:**48–77.
30. Caturegli P, Hejazi M, Suzuki K, Dohan O, Carrasco N, Kohn LD, Rose NR 2000 Hypothyroidism in transgenic mice expressing IFN-gamma in the thyroid. Proc Natl Acad Sci U S A **97:**1719–1724.
31. Kimura H, Tzou SC, Rocchi R, Kimura M, Suzuki K, Parlow AF, Rose NR, Caturegli P 2005 Interleukin (IL)-12-driven primary hypothyroidism: the contrasting roles of two Th1 cytokines (IL-12 and interferon-γ). Endocrinology **146:**3642–3651.
32. Yu S, Fang Y, Sharp GC, Braley-Mullen H 2010 Transgenic expression of TGF-β on thyrocytes inhibits development of spontaneous autoimmune thyroiditis and increases regulatory T cells in thyroids of NOD.H-2h4 mice. J Immunol **184:**5352–5359.

33. Costagliola S, Many MC, Denef JF, Pohlenz J, Refetoff S, Vassart G 2000 Genetic immunization of outbred mice with thyrotropin receptor cDNA provides a model of Graves' disease. J Clin Invest **105:**803–811.
34. Dogan R-NE, Vasu C, Holterman MJ, Prabhakar BS 2003 Absence of IL-4, and not suppression of the Th2 response, prevents development of experimental autoimmune Graves' disease. J Immunol **170:**2195–2204.
35. Nagayama Y, Mizuguchi H, Hayakawa T, Niwa M, McLachlan SM, Rapoport B 2003 Prevention of autoantibody-mediated Graves'-like hyperthyroidism in mice with IL-4, a Th2 cytokine. J Immunol **170:**3522–3527.
36. Ledent C, Dumont JE, Vassart G, Parmentier M 1992 Thyroid expression of an A2 adenosine receptor transgene induces thyroid hyperplasia and hyperthyroidism. EMBO J **11:**537–542.
37. Poll A V, Pierreux CE, Lokmane L, Achouri Y, Jacquemin P, Rousseau GG, Cereghini S, Lemaigre FP 2006 A vHNF1/TCF2-HNF6 cascade regulates the transcription factor network that controls generation of pancreatic precursor cells. Diabetes **55:**61–69.
38. Joshi MU, Pittman HK, Haisch CE, Verbanac KM 2008 Real-time PCR to determine transgene copy number and to quantitate the biolocalization of adoptively transferred cells from EGFP-transgenic mice. Biotechniques **45:**247–258.
39. Capparelli R, Cottone C, D'Apice L, Viscardi M, Colantonio L, Lucretti S, Iannelli D 1997 DNA content differences in laboratory mouse strains determined by flow cytometry. Cytometry **29:**261–266.
40. Burniat A, Jin L, Detours V, Driessens N, Goffard JC, Santoro M, Rothstein J, Dumont JE, Miot F, Corvilain B 2008 Gene expression in RET/PTC3 and E7 transgenic mouse thyroids: RET/PTC3 but not E7 tumors are partial and transient models of human papillary thyroid cancers. Endocrinology **149:**5107–5117.
41. Pfaffl MW 2001 A new mathematical model for relative quantification in real-time RT-PCR. Nucleic Acids Res **29:**2003–2007.
42. Perret J, Ludgate M, Libert F, Gerard C, Dumont JE, Vassart G, Parmentier M 1990 Stable expression of the human TSH receptor in CHO cells and characterization of differentially expressing clones. Biochem Biophys Res Commun **171:**1044–1050.
43. Pohlenz J, Maqueem A, Cua K, Weiss RE, Van Sande J, Refetoff S 1999 Improved radioimmunoassay for measurement of mouse thyrotropin in serum: strain differences in thyrotropin concentration and thyrotroph sensitivity to thyroid hormone. Thyroid **9:**1265–1271.
44. Jeker LT, Hejazi M, Burek CL, Rose NR, Caturegli P 1999 Mouse thyroid primary culture. Biochem Biophys Res Commun **257:**511–515.
45. Senou M, Costa MJ, Massart C, Thimmesch M, Khalifa C, Poncin S, Boucquey M, Gerard AC, Audinot JN, Dessy C, Ruf J, Feron O, Devuyst O, Guiot Y, Dumont JE, Van Sande J, Many MC 2009 Role of caveolin-1 in thyroid phenotype, cell homeostasis, and hormone synthesis: *in vivo* study of caveolin-1 knockout mice. Am J Physiol Endocrinol Metab **297:**438–451.
46. Jacques T, Picard N, Miller RL, Riemondy KA, Houillier P, Sohet F, Ramakrishnan SK, Busst CJ, Jayat M, Corniere N, Hassan H, Aronson PS, Hennings JC, Hubner CA, Nelson RD, Chambrey R, Eladari D 2013 Overexpression of Pendrin in intercalated cells produces chloride-sensitive hypertension. J Am Soc Nephrol **24:**1104–1113.
47. Bénard B, Brault J 1971 Production of peroxide in the thyroid. Union Med Can **100:**701–705.
48. Coelho LP 2013 Mahotas: Open source software for scriptable computer vision. J Open Res Softw **1:**1–7.
49. Van Sande J, Lamy F, Lecocq R, Mirkine N, Rocmans P, Cochaux P, Mockel J, Dumont JE 1988 Pathogenesis of autonomous thyroid nodules: *in vitro* study of iodine and adenosine 3′,5′-monophosphate metabolism. J Clin Endocrinol Metab **66:**570–579.
50. Massart C, Hoste C, Virion A, Ruf J, Dumont JE, Van Sande J 2011 Cell biology of H2O2 generation in the thyroid: investigation of the control of dual oxidases (DUOX) activity in intact *ex vivo* thyroid tissue and cell lines. Mol Cell Endocrinol **343:**32–44.
51. Di Cosmo C, Liao XH, Dumitrescu AM, Philp NJ, Weiss RE, Refetoff S 2010 Mice deficient in MCT8 reveal a mechanism regulating thyroid hormone secretion. J Clin Invest **120:**3377–3388.
52. Huang DW, Sherman BT, Lempicki RA 2009 Systematic and integrative analysis of large gene lists using DAVID bioinformatics resources. Nat Protoc **4:**44–57.
53. Huang DW, Sherman BT, Lempicki RA 2009 Bioinformatics enrichment tools: paths toward the comprehensive functional analysis of large gene lists. Nucleic Acids Res **37:**1–13.
54. Vella V, Mineo R, Frasca F, Mazzon E, Pandini G, Vigneri R, Belfiore A 2004 Interleukin-4 stimulates papillary thyroid cancer cell survival: implications in patients with thyroid cancer and concomitant Graves' disease. J Clin Endocrinol Metab **89:**2880–2889.
55. Kandasamy K, Mohan SS, Raju R, Keerthikumar S, Kumar GSS, Venugopal AK, Telikicherla D, Navarro JD, Mathivanan S, Pecquet C, Gollapudi SK, Tattikota SG, Mohan S, Padhukasahasram H, Subbannayya Y, Goel R, Jacob HKC, Zhong J, Sekhar R, Nanjappa V, Balakrishnan L, Subbaiah R, Ramachandra YL, Rahiman BA, Prasad TSK, Lin JX, Houtman CD, Desiderio S, Renauld JC, Constantinescu SN, Ohara O, Hirano T, Kubo M, Singh S, Khatri P, Draghici S, Bader GD, Sander C, Leonard WJ, Pandey A 2010 NetPath: a public resource of curated signal transduction pathways. Genome Biol **11:**1–9.
56. Chida D, Wakao H, Yoshimura A, Miyajima A 1998 Transcriptional regulation of the beta-casein gene by cytokines: cross-talk between STAT5 and other signaling molecules. Mol Endocrinol **12:**1792–1806.
57. Pedemonte N, Caci E, Sondo E, Caputo A, Rhoden K, Pfeffer U, Di Candia M, Bandettini R, Ravazzolo R, Zegarra-Moran O, Galietta LJ V 2007 Thiocyanate transport in resting and IL-4-stimulated human bronchial epithelial cells: role of Pendrin and anion channels. J Immunol **178:**5144–5153.
58. David M, Ford D, Bertoglio J, Maizel AL, Pierre J 2001 Induction of the IL-13 receptor alpha2-chain by IL-4 and IL-13 in human keratinocytes: involvement of STAT6, ERK and p38 MAPK pathways. Oncogene **20:**6660–6668.
59. Van Staveren WCG, Solís DW, Delys L, Duprez L, Andry G, Franc B, Thomas G, Libert F, Dumont JE, Detours V, Maenhaut C 2007 Human thyroid tumor cell lines derived from different tumor types present a common dedifferentiated phenotype. Cancer Res **67:**8113–8120.
60. Ameziane-El-Hassani R, Talbot M, de Souza Dos Santos MC, Al Ghuzlan A, Hartl D, Bidart JM, De Deken X, Miot F, Diallo I, de Vathaire F, Schlumberger M, Dupuy C 2015 NADPH oxidase DUOX1 promotes long-term persistence of oxidative stress after an exposure to irradiation. Proc Natl Acad Sci **112:**5051–5056.

61. Pachucki J, Wang D, Christophe D, Miot F 2004 Structural and functional characterization of the two human ThOX/Duox genes and their 5′-flanking regions. Mol Cell Endocrinol **214:**53–62.
62. Nofziger C, Dossena S, Suzuki S, Izuhara K, Paulmichl M 2011 Pendrin function in airway epithelia. Cell Physiol Biochem **28:**571–578.
63. Kopp P, Pesce L, Solis-S JC 2008 Pendred syndrome and iodide transport in the thyroid. Trends Endocrinol Metab **19:**260–268.
64. Wangemann P, Kim HM, Billings S, Nakaya K, Li X, Singh R, Sharlin DS, Forrest D, Marcus DC, Fong P 2009 Developmental delays consistent with cochlear hypothyroidism contribute to failure to develop hearing in mice lacking Slc26a4/pendrin expression. Am J Physiol Renal Physiol **297:**1435–1447.
65. Pesce L, Bizhanova A, Caraballo JC, Westphal W, Butti ML, Comellas A, Kopp P 2012 TSH regulates pendrin membrane abundance and enhances iodide efflux in thyroid cells. Endocrinology **153:**512–521.
66. Nofziger C, Vezzoli V, Dossena S, Schönherr T, Studnicka J, Nofziger J, Vanoni S, Stephan S, Silva ME, Meyer G, Paulmichl M 2011 STAT6 links IL-4/IL-13 stimulation with Pendrin expression in asthma and chronic obstructive pulmonary disease. Clin Pharmacol Ther **90:**399–405.
67. Kuperman DA, Lewis CC, Woodruff PG, Rodriguez MW, Yee HY, Dolganov GM, Fahy JV, Erle DJ 2005 Dissecting asthma using focused transgenic modeling and functional genomics. J Allergy Clin Immunol **116:**305–311.
68. Derscheid RJ, van Geelen A, Berkebile AR, Gallup JM, Hostetter SJ, Banfi B, McCray PB, Ackermann MR 2014 Increased concentration of iodide in airway secretions is associated with reduced respiratory syncytial virus disease severity. Am J Respir Cell Mol Biol **50:**389–397.
69. Geiszt M, Leto TL 2004 The Nox family of NADPH oxidases: host defense and beyond. J Biol Chem **279:**51715–51718.
70. Arriagada AA, Albornoz E, Opazo MC, Becerra A, Vidal G, Fardella C, Michea L, Carrasco N, Simon F, Elorza AA, Bueno SM, Kalergis AM, Riedel CA 2015 Excess iodide induces an acute inhibition of the sodium/iodide symporter in thyroid male rat cells by increasing reactive oxygen species. Endocrinology **156:**1540–1551.
71. Gnidehou S, Caillou B, Talbot M, Ohayon R, Kaniewski J, Noël-Hudson MS, Morand S, Agnangji D, Sezan A, Courtin F, Virion A, Dupuy C 2004 Iodotyrosine dehalogenase 1 (DEHAL1) is a transmembrane protein involved in the recycling of iodide close to the thyroglobulin iodination site. FASEB J **18:**1574–1576.
72. Nève P, Rondeaux P 1991 Age-related accumulation of lysosomes and other cytological features in active thyroid follicles of the CBA mouse. Cell Tissue Res **265:**275–285.
73. Twyffels L, Massart C, Golstein PE, Raspe E, Van Sande J, Dumont JE, Beauwens R, Kruys V 2011 Pendrin: the thyrocyte apical membrane iodide transporter? Cell Physiol Biochem **28:**491–496.
74. Fischer H 2009 Mechanisms and function of DUOX in epithelia of the lung. Antioxid Redox Signal **11:**2453–2465.
75. Read ML, Lewy GD, Fong JCW, Sharma N, Seed RI, Smith VE, Gentilin E, Warfield A, Eggo MC, Knauf JA, Leadbeater WE, Watkinson JC, Franklyn JA, Boelaert K, McCabe CJ 2011 Proto-oncogene PBF/PTTG1IP regulates thyroid cell growth and represses radioiodide treatment. Cancer Res **71:**6153–6164.
76. Yap AS, Armstrong JW, Cragoe EJJ, Bourke JR, Huxham GJ, Manley SW 1991 Regulation of thyroid follicular volume by bidirectional transepithelial ion transport. Mol Cell Endocrinol **82:**1–5.
77. Rapoport B, McLachlan SM 2014 Graves' hyperthyroidism is antibody-bediated but is predominantly a Th1-type cytokine disease. J Clin Endocrinol Metab **99:**4060–4061.
78. Heuer M, Aust G, Ode-Hakim S, Scherbaum WA 1996 Different cytokine mRNA profiles in Graves' disease, Hashimoto's thyroiditis, and nonautoimmune thyroid disorders determined by quantitative reverse transcriptase polymerase chain reaction (RT-PCR). Thyroid **6:**97–106.
79. Lee YJ, Huang CY, Ting WH, Lee HC, Guo WL, Chen WF, Lin CL, Liu HF, Lin M, Lo FS 2011 Association of an IL-4 gene haplotype with Graves disease in children: experimental study and meta-analysis. Hum Immunol **72:**256–261.
80. Song R, Qin Q, Wang X, Yan N, Meng S, Shi X, He S, Zhang J 2016 Differential cytokine expression detected by protein microarray screening in peripheral blood of patients with refractory Graves' disease. Clin Endocrinol (Oxf) **84:**402–407.
81. Chen CR, Aliesky H, Pichurin PN, Nagayama Y, McLachlan SM, Rapoport B 2004 Susceptibility rather than resistance to hyperthyroidism is dominant in a thyrotropin receptor adenovirus-induced animal model of Graves' disease as revealed by BALB/c-C57BL/6 hybrid mice. Endocrinology **145:**4927–4933.
82. Rapoport B, Aliesky HA, Banuelos B, Chen C, McLachlan SM 2015 A unique mouse strain that develops spontaneous, iodine-accelerated, pathogenic antibodies to the human thyrotrophin receptor. J Immunol **194:**4154–4161.
83. Royaux IE, Suzuki K, Mori A, Katoh R, Everett LA, Kohn LD, Green ED 2000 Pendrin, the protein encoded by the pendred syndrome gene (PDS), is an apical porter of iodide in the thyroid and is regulated by thyroglobulin in FRTL-5 cells. Endocrinology **141:**839–845.
84. Bidart JM, Mian C, Lazar V, Russo D, Filetti S, Caillou B, Schlumberger M 2000 Expression of pendrin and the Pendred syndrome (PDS) gene in human thyroid tissues. J Clin Endocrinol Metab **85:**2028–2033.
85. Kondo T, Ezzat S, Asa SL 2006 Pathogenetic mechanisms in thyroid follicular-cell neoplasia. Nat Rev Cancer **6:**292–306.
86. Skubis-Zegadło J, Nikodemska A, Przytuła E, Mikula M, Bardadin K, Ostrowski J, Wenzel BE, Czarnocka B 2005 Expression of pendrin in benign and malignant human thyroid tissues. Br J Cancer **93:**144–151.
87. Yoshida A, Hisatome I, Taniguchi S, Shirayoshi Y, Yamamoto Y, Miake J, Ohkura T, Akama T, Igawa O, Shigemasa C, Kamijo K, Ikuyama S, Caturegli P, Suzuki K 2009 Pendrin is a novel autoantigen recognized by patients with autoimmune thyroid diseases. J Clin Endocrinol Metab **94:**442–448.
88. Kacem HH, Rebai A, Kaffel N, Masmoudi S, Abid M, Ayadi H 2003 PDS is a new susceptibility gene to autoimmune thyroid diseases: association and linkage study. J Clin Endocrinol Metab **88:**2274–2280.

Address correspondence to:
Zineb Eskalli, PhD
ULB—IRIBHM
Local C4-145, Batiment C
808 Route de Lennik
1070 Brussels
Belgium

E-mail: Zineb.Eskalli@ulb.ac.be